Journal of ELECTRONIC MATERIALS, Vol. 48, No. 5, 2019
https://doi.org/10.1007/s11664-019-07031-x

TOPICAL COLLECTION: 60TH ELECTRONIC MATERIALS CONFERENCE 2018

GaN Heteroepitaxy on Strain-Engineered (111) Si/$Si_{1-x}Ge_x$

ANUSHKA BANSAL,[1] NATHAN C. MARTIN,[1] KE WANG,[2] and JOAN M. REDWING[1,3,4]

1.—Department of Materials Science and Engineering, Pennsylvania State University, University Park, PA 16802, USA. 2.—Materials Characterization Laboratory, University Park, PA 16802, USA. 3.—Materials Research Institute, Pennsylvania State University, University Park, PA 16802, USA. 4.—e-mail: jmr31@psu.edu

The metalorganic chemical vapor deposition growth of GaN on strained Si/$Si_{1-x}Ge_x$ epilayers on (111) Si substrates was investigated. A multi-beam optical stress sensor (MOSS) was used for *in situ* stress measurements during growth of the entire heterostructure. MOSS was initially used to measure the extent of stress relaxation during the growth of constant-composition $Si_{1-x}Ge_x$ layers on Si. The results compared favorably to that obtained by post-growth high-resolution x-ray diffraction. MOSS was also used to monitor stress during the growth of thin, tensile-strained Si on relaxed $Si_{0.95}Ge_{0.05}$/compositionally graded epilayers. The tensile-strained Si/$Si_{1-x}Ge_x$ epilayers were then used as virtual substrates for the growth of GaN epilayers using a thin (90 nm) AlN buffer layer. GaN grown on tensile-strained Si exhibited a higher initial compressive stress and reduced final tensile stress compared to films grown directly on (111) Si, resulting in a lower crack density in the GaN along with a reduced density of threading dislocations. These results suggest that strain engineering of the Si surface prior to growth may provide an alternative method to improve the quality of GaN grown on (111) Si.

Key words: Metalorganic chemical vapor deposition, GaN, *in situ* stress, silicon–germanium, threading dislocation density, crack density

INTRODUCTION

Group III nitrides are an important class of wide-bandgap semiconductors for solid-state lighting, high-frequency power electronics and vertical power switching devices.[1–3] The growth of GaN and other related nitrides on Si substrates is desired both to take advantage of the large wafer size and low cost as well as the potential to integrate these devices with Si-based integrated circuits. However, due to the heteroepitaxial mode of growth for GaN on (111) Si, these films typically suffer from substantial lattice mismatch which gives rise to a higher density of threading dislocations (10^8–10^{10} cm^{-2}) and introduces tensile growth stress.[4] In addition, the coefficient of thermal expansion (CTE) mismatch between GaN and (111) Si induces additional tensile stress into the film after cooldown from the growth temperature.[5,6] The tensile stress is relaxed by brittle fracture, resulting in the formation of channeling cracks in the film which are detrimental to device fabrication.

There are many approaches to mitigate tensile stress in GaN films grown on (111) Si. The general strategy involves strain engineering to introduce compressive epitaxial mismatch stress within the structure to offset the tensile stress arising from growth and CTE mismatch.[5] This is typically done by adding AlN interlayers,[6] AlN/GaN superlattices,[7] SiN_x layers[8] and compositionally graded AlGaN transition layers.[9,10] These methods have been shown to reduce the crack density as well as the threading dislocation (TD) density in the GaN films.[5] However, addition of thick, high-Al-fraction layers within the layer structure can be problematic due to the wider bandgap and higher resistivity of

(Received October 17, 2018; accepted January 31, 2019; published online February 21, 2019)

$Al_xGa_{1-x}N$ and the possibility of deep-level states which are undesired particularly for vertical devices.

An alternative approach to strain engineering for GaN growth on Si is to modify the stress in the Si substrate prior to group III nitride growth. For example, previous work demonstrated the use of N^+ ion implantation into AlN/(111) Si substrates to form a buried defective layer within the substrate that resulted in a reduction in the initial compressive stress and lower overall growth stress and film cracking in the subsequent GaN films.[11–14] In this study, a related substrate engineering method was investigated involving tensile-strained (111) Si grown on relaxed lattice-mismatched $Si_{1-x}Ge_x$ epilayers which were used as "virtual substrates" for GaN growth. The $Si/Si_{1-x}Ge_x$ heterostructures were grown *in situ* in the metalorganic chemical vapor deposition (MOCVD) reactor to provide a pristine surface for subsequent growth of group III nitride layers. *In situ* wafer curvature measurements were used to monitor the extent of stress relaxation in the graded $Si_{1-x}Ge_x$ layers, measure the tensile strain in the top Si layer and study the evolution of growth stress in the subsequent AlN/GaN layers. The GaN layers grown on the tensile-strained $Si/Si_{1-x}Ge_x$ exhibited a lower TD density and reduced tensile stress during growth which lead to a reduction in the density of channeling cracks compared to comparable layers grown on (111) Si.

EXPERIMENTAL PROCEDURE

The Si substrates used for the growth were cleaned by 10-min immersion in 10:1 hydrofluoric acid (HF) after the organics removal step to remove any native oxide present on the surface. The growths were performed in a custom-designed vertical quartz tube MOCVD reactor that includes an inductively heated SiC-coated graphite susceptor. Initial studies focused on the development of strained $Si/Si_{1-x}Ge_x$ epilayers employing a multi-beam optical stress sensor (MOSS) to measure compressive stress relaxation in the $Si_{1-x}Ge_x$ layers and tensile stress in the Si cap layer. SiH_4 (10% in H_2) and GeH_4 (2% in H_2) were used as precursors to enable the growth of $Si/Si_{1-x}Ge_x$ heterostructures. These growths were performed at a temperature of 1150°C and a total pressure of 1.33 kPa using a constant SiH_4 flow rate of 219.9 μmol/min and GeH_4 flow rates that varied from 4.46 μmol/min to 8.93 μmol/min depending on the $Si_{1-x}Ge_x$ composition (x = 0.05–0.10). These virtual substrates were then used to study the effects of strained Si on the nucleation and subsequent epitaxial growth of AlN/GaN. Precursor sources for the nitride growth included trimethylaluminum (TMAl), trimethylgallium (TMGa) and ultra-high-purity ammonia (NH_3) for Al, Ga and N sources, respectively with hydrogen as a carrier gas. Initially, a thin layer of AlN (90 nm) was deposited on top of strained Si and then a $\sim$ 1-μm-thick GaN layer was deposited. During AlN/GaN growth, the reactor was held at a constant pressure of 6.67 kPa, while the temperature of the susceptor was maintained at 1150°C. The AlN buffer layers were deposited using TMA and NH_3 flow rates of 10.3 μmol/min and 89.3 mmol/min, respectively. The GaN film was deposited using TMGa and NH_3 flow rates of 6.8 μmol/min and 89.3 mmol/min, respectively. A key point to note here is that the entire stack was deposited sequentially in the MOCVD reactor, and the sample surface was not exposed to atmosphere between the strained $Si/Si_{1-x}Ge_x$ and GaN growth.

To monitor the stress evolution in the films, k-Space Associates (kSA) MOSS was employed for *in situ* wafer curvature measurements of the films during the growth process. It employs a free-standing substrate and a linear array of reflected laser beams, as shown in the inset of Fig. 1a, to obtain information on curvature changes of the substrate. The curvature data can be converted to the product of the film stress (σ_f) and the film thickness (h_f) via a modified Stoney's equation[15,16] which relates stress-thickness product ($\sigma_f h_f$) of the thin film to the sample curvature (κ) using the following relation:

$$\sigma_f h_f = \frac{M_s h_s^2}{6}\kappa \qquad (1)$$

where h_s is the substrate thickness and M_s is the substrate biaxial modulus (170 GPa).

High-resolution x-ray diffraction (HRXRD) was performed using a Philips MRD four-circle diffractometer with CuKα radiation to measure the post-growth strain and composition of the $Si_{1-x}Ge_x$ films (using reciprocal space maps) along with an estimate of the TD densities in the GaN film. The $Si_{1-x}Ge_x$ unstrained lattice parameter varies non-linearly with the Ge content of the $Si_{1-x}Ge_x$ films; therefore, the following equation was used rather than a Vegard's Law approximation to calculate the predicted lattice parameter of the $Si_{1-x}Ge_x$ films[17]:

$$a(x) = 5.4309 + 0.200326x + 0.026274x^2 \qquad (2)$$

The elastic constants as well as the lattice parameters used in the calculations were room-temperature values.[18]

Cross-section samples for transmission electron microscopy (TEM) analysis were prepared using an FEI Helios 660 focused ion beam (FIB) system. A thick protective amorphous carbon layer was deposited over the region of interest, then Ga+ ions (30 kV then stepped down to 1 kV to avoid ion beam damage to the sample surface) were used in the FIB to make the samples electron-transparent for TEM images. The high-resolution TEM imaging was performed in an FEI dual-aberration-corrected Titan3 G2 60-300 S/TEM at 200 kV. Energy dispersive x-ray spectroscopy (EDS) mapping of the entire stack was performed using the SuperX EDS system under scanning TEM (STEM) mode. Optical

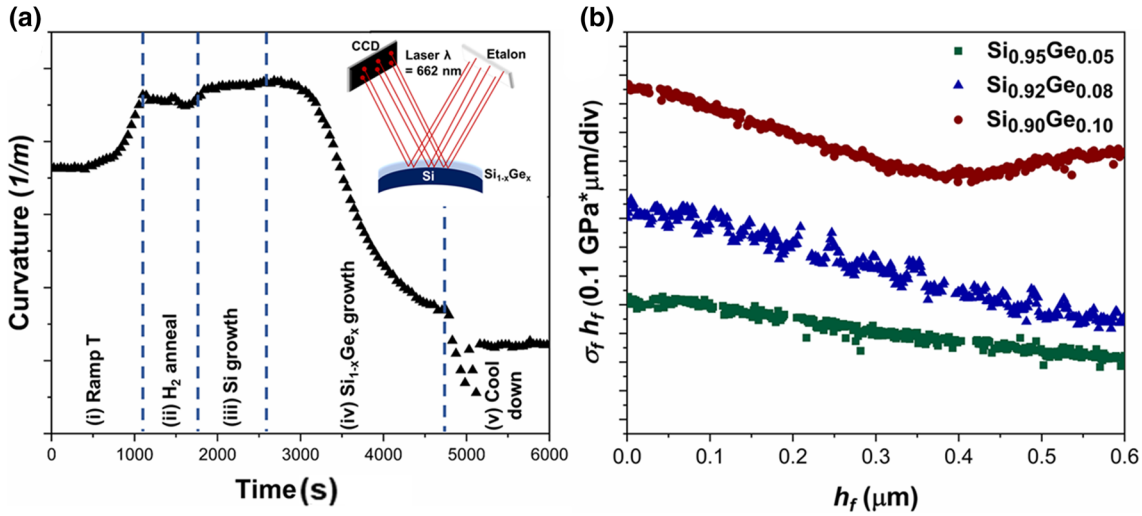

Fig. 1. (a) MOSS curvature data measured during the entire growth process for Si/$Si_{0.95}Ge_{0.05}$ and (inset) schematic of MOSS setup showing the effect of substrate curvature on the reflected laser spots. (b) $\sigma_f h_f$ versus h_f plots obtained during growth of $Si_{1-x}Ge_x$ segments with different compositions.

microscopy was performed to qualitatively evaluate the crack density of the GaN film surfaces.

RESULTS AND DISCUSSION

Stress relaxation during growth of $Si_{1-x}Ge_x$ ($0 < x < 0.10$) on (100) Si was initially investigated to compare the results obtained *in situ* by MOSS with that provided by post-growth HRXRD. A graph of the relative curvature of the sample measured during the growth of $Si_{0.95}Ge_{0.05}$ on Si is shown in Fig. 1a as an example of the raw data obtained using the MOSS. In the first segment (1), the Si substrate was heated to the growth temperature (1150°C) and the wafer bows upward (concave) due to the thermal gradient between the bottom of the wafer that is in contact with the heated susceptor and the top of the wafer that is exposed to the cooler gas ambient.[19] In the H_2 anneal segment (2), the substrate is kept at a constant temperature under the H_2 ambient to remove any residual oxide. Since there is no deposition on the substrate during this step, the curvature remains relatively constant. After high-temperature annealing of the substrate, a thin layer (600 nm) of Si was deposited on the Si substrate (3) to provide a higher-quality surface for further growth of the $Si_{1-x}Ge_x$ film. Since there is no lattice mismatch between substrate and film, there was no observed curvature change in MOSS as indicated. The next growth segment (4) involves deposition of $Si_{1-x}Ge_x$. Due to epitaxial lattice mismatch between $Si_{1-x}Ge_x$ and Si, the film initially grows under a compressive stress, giving rise to a negative curvature. As the growth proceeds, the compressive stress begins to relax, as can be seen from the slope change with time in the plot. During the post-growth cooling step (5), the wafer bows downward in the opposite direction of step (1) as the thermal gradient between the top and bottom of the wafer is reduced. The net change in curvature between steps (1) and (5) is indicative of the residual compressive stress due in the $Si_{1-x}Ge_x$ layer.

A series of constant-composition $Si_{1-x}Ge_x$ samples (x = 0.05, 0.08, 0.10) were grown using a similar process. The stress-thickness versus thickness curves calculated during growth of the $Si_{1-x}Ge_x$ (x = 0.05, 0.08, 0.10) layers (segment iv) are shown in Fig. 1b. In all cases, the stress-thickness curve has a short initial flat segment, which is likely due to the time delay between the actuation of the GeH_4 source valve and the incorporation of Ge in the growing surface. Following this segment, the slope of the stress-thickness versus thickness curves becomes negative, indicating that the $Si_{1-x}Ge_x$ films are growing under a nearly constant initial compressive stress which arises from the epitaxial mismatch between $Si_{1-x}Ge_x$/Si. For the series of samples, the initial slope of the plot becomes more negative as the GeH_4 flow rate (and hence Ge content) increases. The corresponding values of the initial compressive stress obtained from the MOSS are included in Table I. As the film thickness increases, the compressive stress begins to relax, which is indicated by the change in the slope of the curve. For the $Si_{0.95}Ge_{0.05}$ film, the slope of the stress-thickness curve does not change significantly with thickness, indicating minor stress relaxation. The $Si_{0.92}Ge_{0.08}$ and $Si_{0.90}Ge_{0.10}$ samples, by contrast, exhibit more pronounced change in slope. In case of the $Si_{0.90}Ge_{0.10}$ sample, after a thickness of $\sim$ 400 nm, the compressive stress in the film gradually relaxes and evolves into a tensile stress. The reason for this behavior is not fully understood, but correlates with changes in surface roughness associated with the stress relaxation process.

Table I includes a comparison of the initial incremental stress present in the $Si_{1-x}Ge_x$ films at the growth temperature of 1150°C as measured by the MOSS, the post-growth stress at room temperature

as measured by HRXRD and the predicted epitaxial stress in the film based on the lattice mismatch between film and substrate. The compressive stress obtained from the MOSS measurement is slightly lower than that predicted by epitaxial mismatch. The differences can likely be attributed to the fact that the MOSS measurements were obtained at the growth temperature of 1150°C, while the predicted values assume room temperature. Furthermore, the post-growth stress measurement by HRXRD measures the mean stress in the film which includes stress relaxation that occurs during growth and cooldown. As a result, the film stress measured by HRXRD is lower than both the values measured by the MOSS and those predicted based on epitaxial mismatch.

To achieve a thin tensile-strained Si layer, the common approach is to gradually relax the compressive stress in the $Si_{1-x}Ge_x$ via compositional grading. Prior research carried out on $Si_{1-x}Ge_x$/Si heterostructures demonstrated that as the composition is gradually changed to $Si_{1-x}Ge_x$ from Si, the rate of dislocation nucleation is minimized while the rate of dislocation glide is simultaneously maximized.[20] Therefore, before depositing a constant-composition $Si_{0.95}Ge_{0.05}$ layer, a graded $Si_{1-x}Ge_x$ layer with continuous composition grading from $Si_{0.98}Ge_{0.02}$ to $Si_{0.95}Ge_{0.05}$ was deposited as shown in the inset of Fig. 2a. The MOSS was also used to monitor the evolution of stress during the growth of the compositionally graded and constant-composition $Si_{1-x}Ge_x$ layers and measure the tensile strain in the top Si layer. Figure 2a shows the stress-thickness versus thickness plot for the entire stack up to the thin layer of strained Si on the top. To better understand the stress relaxation in the $Si_{1-x}Ge_x$ films, the derivative of the stress-thickness versus thickness curve was calculated which provides the incremental stress in the film as the growth progresses (Fig. 2b). As can be seen from Fig. 2b, the film stress is initially zero (due to the time delay mentioned previously) and then transitions into a compressive stress upon incorporation of Ge in the film. The compressive stress in the compositionally graded $Si_{1-x}Ge_x$ layer gradually relaxes from − 0.33 GPa to − 0.15 GPa. As growth proceeds, the compressive stress in the constant-composition $Si_{0.95}Ge_{0.05}$ film relaxes and transitions to a small tensile stress of 0.16 GPa. The GeH_4 was then switched out of the inlet gas stream to grow a thin (∼ 100 nm) Si layer. As shown in Fig. 2a, the slope of the stress-thickness versus thickness curve abruptly becomes positive which corresponds to an incremental tensile stress of 0.28 GPa (Fig. 2b). The

Table I. Comparison of $Si_{1-x}Ge_x$ film stress measured *in situ* using a MOSS, *ex situ* using HRXRD and predicted epitaxial stress based on lattice mismatch using film composition determined by HRXRD

Film composition (HRXRD)	Initial stress (GPa, MOSS)	Mean stress (GPa, HRXRD)	Epitaxial stress (GPa, predicted)
$Si_{0.95}Ge_{0.05}$	− 0.33 ± 0.03	− 0.31	− 0.36
$Si_{0.92}Ge_{0.08}$	− 0.54 ± 0.07	− 0.51	− 0.58
$Si_{0.90}Ge_{0.10}$	− 0.68 ± 0.04	− 0.65	− 0.72

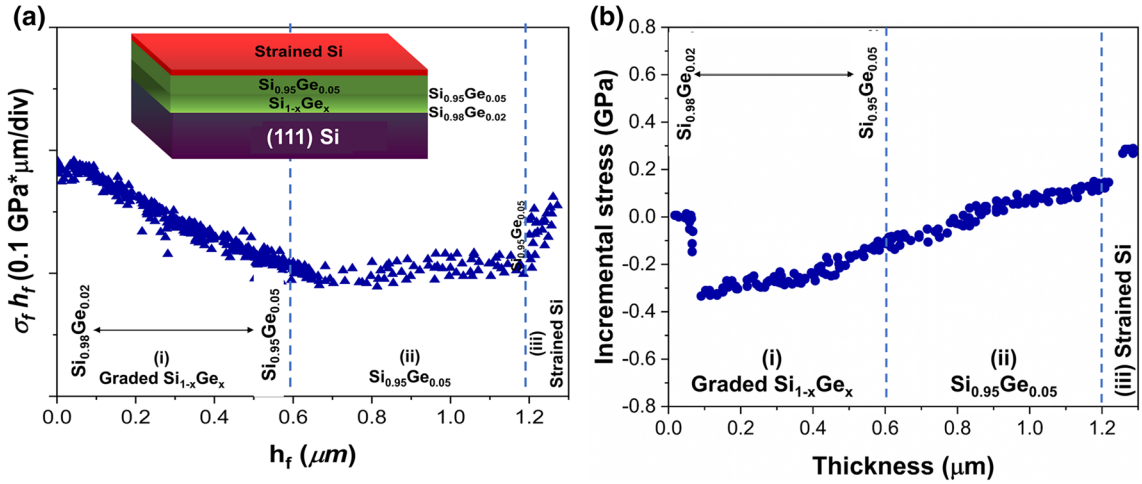

Fig. 2. (a) $\sigma_f h_f$ versus h_f plot and (b) corresponding incremental stress versus thickness measured as $Si_{1-x}Ge_x$ composition is initially graded from $Si_{0.98}Ge_{0.02}$ to $Si_{0.95}Ge_{0.05}$ followed by growth of a 600-nm constant-composition $Si_{0.95}Ge_{0.05}$ layer and tensile-strained Si cap layer. The inset in (a) is a schematic of the layer structure.

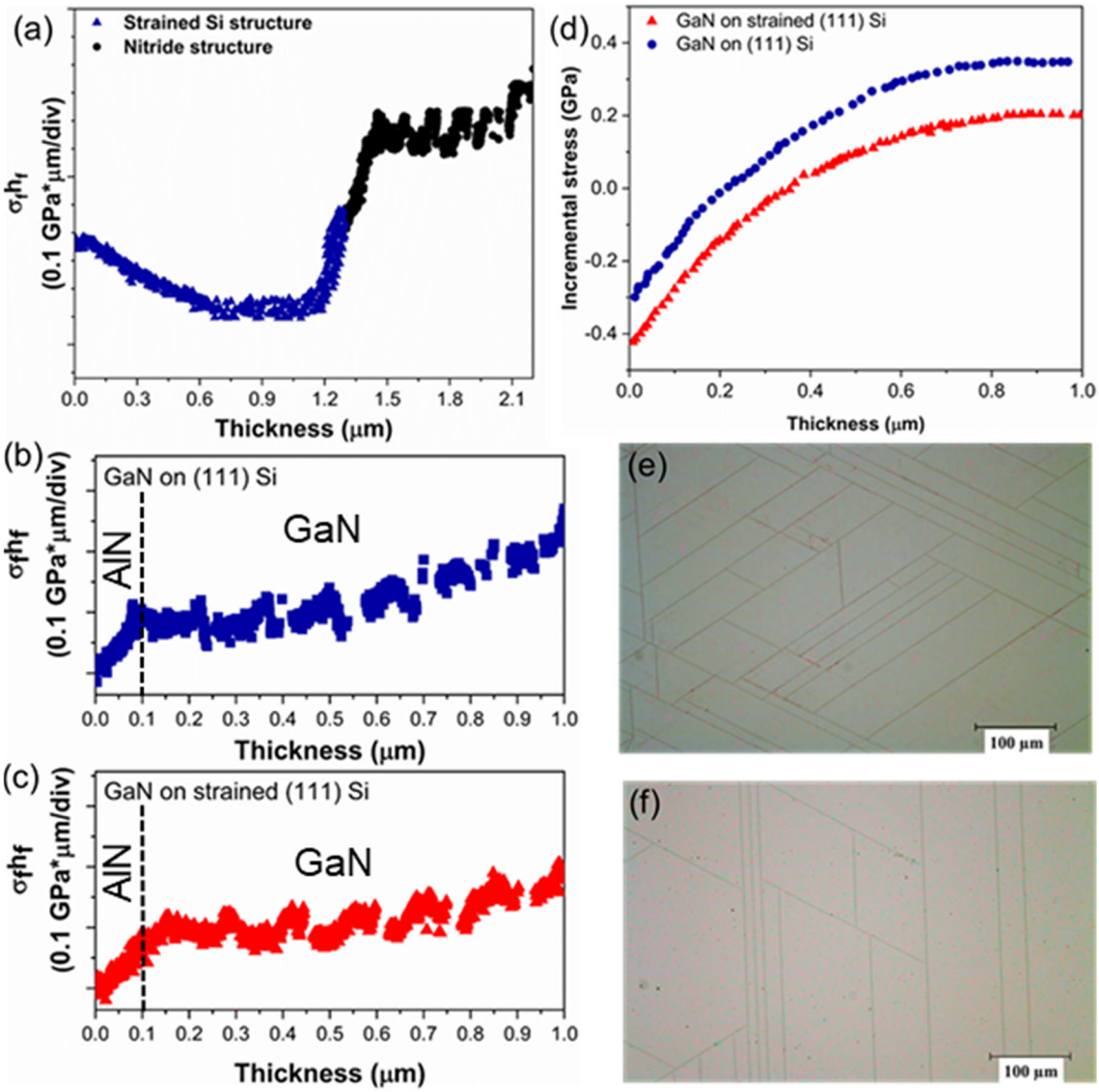

Fig. 3. (a) $\sigma_f h_f$ versus h_f plot measured during the entire stacked structure of $Si_{1-x}Ge_x$/strained Si/AlN/GaN on (111) Si. $\sigma_f h_f$ versus h_f plots measured during AlN/GaN growth on (b) unstrained and (c) strained (111) Si. (d) Incremental stress versus thickness in GaN layer showing higher initial compressive stress and lower final tensile stress in GaN grown on strained (111) Si as compared to GaN on unstrained (111) Si. Nomarski optical micrographs of GaN on (e) unstrained and (f) strained (111) Si.

corresponding amount of strain present in the Si film was calculated to be 0.15%.

The tensile-strained Si/$Si_{1-x}Ge_x$ layers grown on (111) Si were then used as virtual substrates for the growth of GaN, and the results were compared to growth directly on "unstrained" (111) Si. The entire stack was deposited sequentially in the MOCVD reactor such that the sample was not cooled to room temperature or exposed to atmosphere in between the strained Si/$Si_{1-x}Ge_x$ and GaN growth. MOSS data obtained during the entire growth process is shown in Fig. 3a. Figure 3b and c show the stress-thickness versus thickness plots obtained during AlN and GaN growth on unstrained (111) Si and tensile-strained (111) Si, respectively. In both cases, the AlN grows under a constant tensile stress, although the stress in the AlN film was observed to be higher (1.4 GPa) on unstrained (111) Si (Fig. 3b) compared to 1.2 GPa which was measured on the strained (111) Si substrate (Fig. 3c). The GaN then grows on the AlN under a slight initial compressive stress due to epitaxial mismatch which quickly transitions to a tensile stress. The slight oscillations seen in the stress-thickness versus thickness data in Fig. 3a–c are due to beam-steering effects caused by thickness variations in the GaN layer.[21]

To remove the artifacts/oscillations present in the stress-thickness versus thickness data, smoothening was performed before curve fitting and then the derivative was taken to obtain incremental stress in

the film as a function of thickness (Fig. 3d). GaN initiates growth on the AlN on the tensile-strained Si under a larger compressive stress of −0.42 GPa (Fig. 3d) compared to − 0.30 GPa for growth on unstrained Si (111). During GaN growth on (111) Si, the stress transitions from compressive to tensile after ∼ 0.2 μm; however, for the case of growth on strained Si, the stress transition occurs at ∼ 0.4 μm. In both cases, the tensile stress in the GaN evolves to a constant value which is higher (0.35 GPa) for growth on unstrained Si compared to growth on strained Si (0.18 GPa). From the Nomarski optical micrographs shown in Fig. 3e and f, it was observed that the crack density in the GaN film deposited on strained Si is reduced compared to the GaN deposited on unstrained Si. The reduced density of channeling cracks is consistent with the lower tensile stress measured in the GaN grown on the strained (111) Si.

The screw and edge TD density in the GaN layers were estimated from the full width at half maximum (FWHM) of ω scans on GaN (0002) and (10$\bar{1}$0), respectively, by XRD. The rocking curve measurement on the (0002) plane is straightforward. However, the ω scan on (10$\bar{1}$0) typically requires grazing incidence angle XRD (GIXRD) with a high-intensity x-ray source. Here, we used an empirical model considering crystallite rotations and convolutions of two pseudo-Voigt functions that reflect tilt and twist with interdependence parameter m between them, which was developed by Srikant et al.[22] Figure 4 shows the measured FWHMs of ω scans on (0002), (10$\bar{1}$5), (10$\bar{1}$2), (20$\bar{2}$3), (10$\bar{1}$1), and (30$\bar{3}$2), in the GaN on unstrained and strained (111) Si. The FWHM of (10$\bar{1}$0) at 90° can be obtained from the fit (solid line), yielding the twist of GaN. Then, the screw and edge TD density can be estimated from the classical model for randomly distributed dislocations:

$$\rho_{\text{screw}} = \frac{\tau_{\text{tilt}}^2}{4.36 b_{\text{screw}}^2} \tag{3}$$

$$\rho_{\text{edge}} = \frac{\tau_{\text{twist}}^2}{4.36 b_{\text{edge}}^2} \tag{4}$$

where τ_{tilt} and τ_{twist} are the FWHMs of the (0002) and (10$\bar{1}$0) ω scans and b_{screw} (5.1850 Å) and b_{edge} (3.1888 Å) are the Burgers vectors along (0001) and $\frac{1}{3}11\bar{2}0$, respectively. In the two samples, the screw dislocation density remained almost the same (Table II), whereas the edge dislocation density was reduced by a factor of two in the GaN film grown on the tensile-strained Si layer.

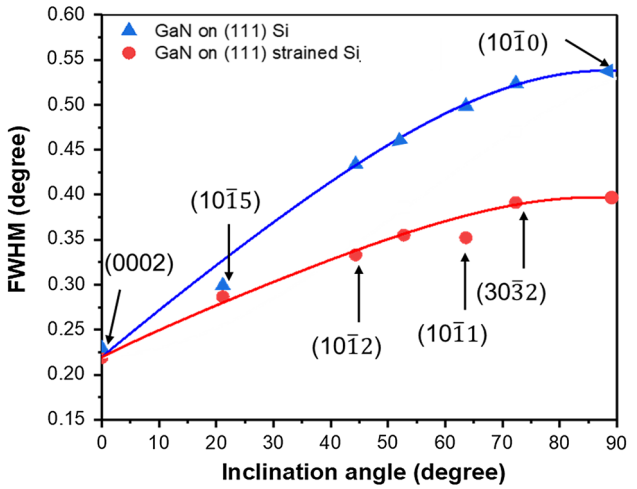

Fig. 4. A series of measured XRC FWHM reflections as a function of inclination angle to estimate tilt and twist at the inclination angle of 0° and 90°, respectively, and calculation of TD density in the GaN films for the growth of GaN on (111) Si: (blue triangles, solid line fit), and GaN on strained (111) Si (red circles, solid line fit) (Color figure online).

Cross-section TEM and STEM EDS mapping were used for microstructural investigation and chemical analysis of the GaN/AlN/Si/$Si_{0.95}Ge_{0.05}$ sample. Figure 5a shows a cross-sectional bright-field TEM image of the entire stacked structure. As can be seen from the micrograph, there were no visible dislocations present in the Si/$Si_{1-x}Ge_x$ heterostructure, likely due to the low Ge fraction. However, dislocations are evidently visible in the AlN/GaN heterostructure. The layered heterostructure including the GaN/AlN layers on the strained Si/$Si_{1-x}Ge_x$ virtual substrate is evident from the EDS compositional map shown in Fig. 5b. The thin tensile-strained Si layer (∼ 30 nm) is present at the interface between the $Si_{0.95}Ge_{0.05}$ and the AlN. The thickness of the Si layer was expected to be ∼ 100 nm based on the growth rate. The lower-than-expected thickness is likely due to diffusion of Ge from the $Si_{0.95}Ge_{0.05}$ layer during the extended exposure to high temperature during growth of the AlN/GaN layers. Figure 5c shows the corresponding high-angle annular dark-field (HAADF) image of the structure where threading dislocations are

Table II. Estimated TD densities of GaN on (111) Si and strained (111) Si as calculated by HRXRD

	Screw ρ_{TD} (cm^{-1})	Edge ρ_{TD} (cm^{-1})	Total ρ_{TD} (cm^{-1})
GaN on Si (111)	5.23×10^8	3.6×10^{10}	3.65×10^{10}
GaN on strained (111) Si	5.11×10^8	1.8×10^{10}	1.85×10^{10}

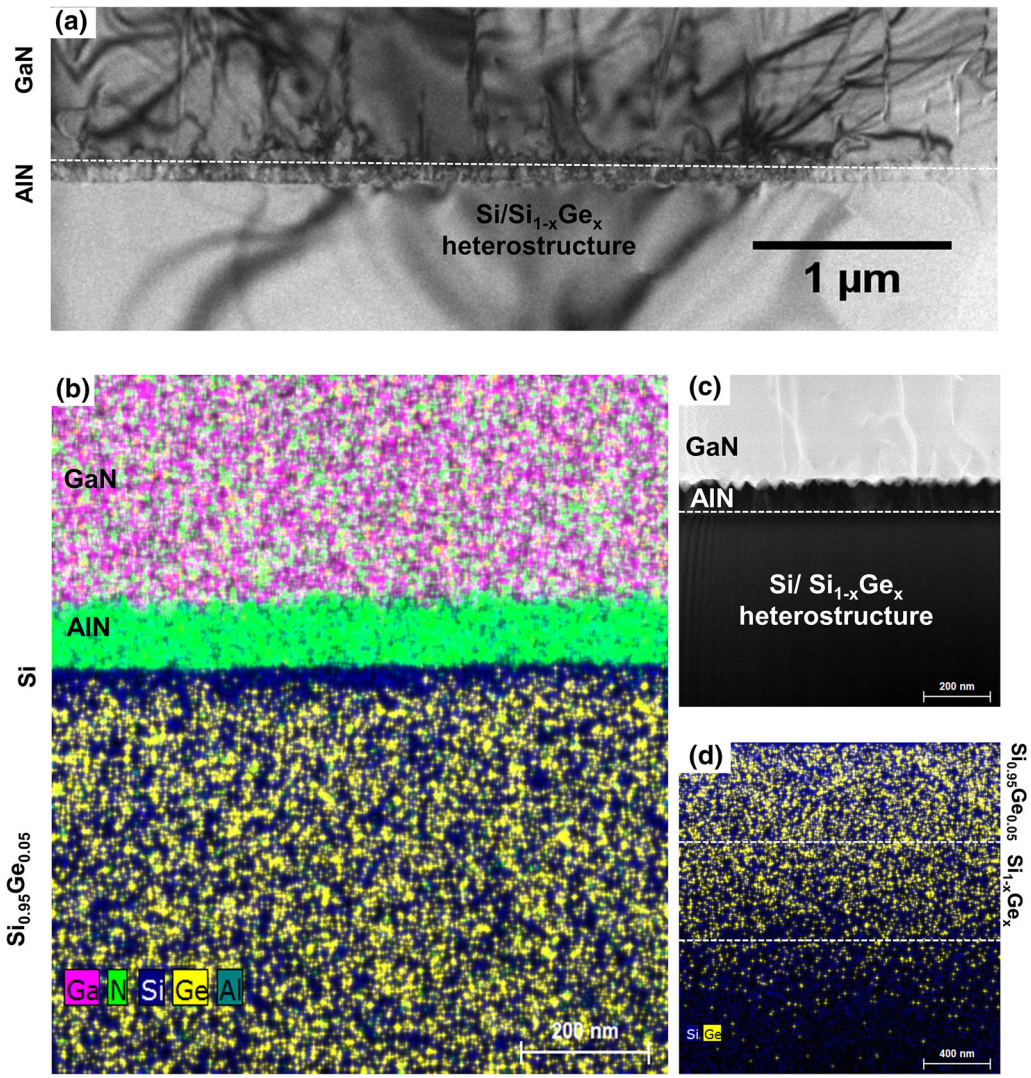

Fig. 5. Microstructure and compositional analysis of GaN/AlN/Si/$Si_{0.95}Ge_{0.05}$ layer structure. (a) Cross-sectional bright-field TEM image of the entire stacked structure. (b) EDS compositional map showing the layered heterostructure including the GaN/AlN layers on the strained Si/$Si_{1-x}Ge_x$ virtual substrate. (c) Corresponding cross-section high-angle annular dark-field (HAADF) TEM image of GaN on AlN/strained Si showing threading dislocations in the GaN film. (d) EDS mapping of the constant-composition $Si_{0.95}Ge_{0.05}$ layer at the top, the graded $Si_{1-x}Ge_x$ layer with x from 0.02 to 0.05 in the middle and the bottom Si layer.

clearly visible in the GaN film. The EDS image in Fig. 5d contains three sections: the constant-composition $Si_{0.95}Ge_{0.05}$ layer at the top, the graded $Si_{1-x}Ge_x$ layer with x from 0.02 to 0.05 in the middle and the bottom Si layer. To confirm the Ge fraction in the compositionally graded $Si_{1-x}Ge_x$ and constant-composition $Si_{1-x}Ge_x$ film, quantitative EDS mapping (Fig. 5d) was performed by using a standardless analysis method. The Ge fraction was found to vary from 2% to 6% in the $Si_{1-x}Ge_x$ layer, which is close to the measurement obtained using HRXRD. However, it is difficult to assess the extent of Ge diffusion that occurred in the graded layer at growth temperatures due to the uneven thickness of the TEM sample.

CONCLUSION

The growth of GaN on tensile-strained Si/$Si_{1-x}Ge_x$ epilayers was demonstrated as an alternative approach to modify growth stress and film cracking. Based on the lattice mismatch between tensile-strained (111) Si (> 3.84 Å) and AlN (3.11 Å) as compared to unstrained (111) Si, a higher tensile stress would be expected in the AlN film grown on strained (111) Si. However, a lower tensile stress (1.2 GPa) was measured in the AlN film on strained (111) Si compared to the unstrained (111) Si substrate (1.4 GPa). The lower tensile stress in the AlN is believed to arise instead from differences in the surface morphology and roughness of the tensile-strained Si (111) surface possibly due to diffusion of

Ge from the underlying $Si_{1-x}Ge_x$ layer during the high-temperature AlN growth step, as can be seen from Fig. 5b. The lower tensile stress in AlN resulted in an increased initial compressive stress in the GaN due to epitaxial mismatch. The higher initial compressive stress in the GaN on tensile-strained (111) Si promotes bending and annihilation of edge-type dislocations,[5] leading to an overall lower TD density and reduced final tensile stress and film cracking in the GaN epilayer. These initial studies were carried out using low-Ge-fraction ($x < 0.10$) $Si_{1-x}Ge_x$ layers to minimize effects of dislocations coming from the Si substrate. Further improvements are therefore anticipated through using layers of higher Ge fraction and optimized $Si/Si_{1-x}Ge_x$ heterostructures.

ACKNOWLEDGMENTS

The authors would like to thank Dr. Tanushree Choudhury for helpful discussions during the experiments. This work was supported by the National Science Foundation under Grants Nos. DMR-1410765 and DMR-1808900.

REFERENCES

1. O. Ambacher, *J. Phys. D Appl. Phys.* 31, 2653 (1998).
2. J. Wu, *J. Appl. Phys.* 106, 11101 (2009).
3. F. Semond, Y. Cordier, N. Grandjean, F. Natali, B. Damilano, and S. Ve, *Phys. Status Solidi* 510, 501 (2001).
4. S. Raghavan and J.M. Redwing, *J. Appl. Phys.* 98, 23514 (2005).
5. J.M. Redwing and S. Raghavan, *III–V Compound Semiconductors: Integration with Silicon-Based Microelectronics*, ed. T. Li, M. Mastro, and A. Dadgar (Boca Raton: CRC Press, 2011).
6. A. Dadgar, J. Bläsing, A. Diez, A. Alam, M. Heuken, and A. Krost, *Jpn. J. Appl. Phys.* 39, L1183 (2000).
7. S. Iwakami, O. Machida, Y. Izawa, R. Baba, M. Yanagihara, T. Ehara, N. Kaneko, H. Goto, and A. Iwabuchi, *Jpn. J. Appl. Phys.* 46, L721 (2007).
8. T. Riemann, T. Hempel, J. Christen, P. Veit, R. Clos, A. Dadgar, A. Krost, U. Haboeck, and A. Hoffmann, *J. Appl. Phys.* 99, 123518 (2006).
9. H. Marchand, L. Zhao, N. Zhang, B. Moran, R. Coffie, U.K. Mishra, J.S. Speck, S.P. DenBaars, and J.A. Freitas, *J. Appl. Phys.* 89, 7846 (2001).
10. S. Raghavan and J. Redwing, *J. Appl. Phys.* 98, 23515 (2005).
11. M. Jamil, J.R. Grandusky, V. Jindal, F. Shahedipour-Sandvik, S. Guha, and M. Arif, *Appl. Phys. Lett.* 87, 82103 (2005).
12. M. Jamil, J.R. Grandusky, V. Jindal, N. Tripathi, and F. Shahedipour-Sandvik, *J. Appl. Phys.* 102, 23701 (2007).
13. J.C. Gagnon, M. Tungare, X. Weng, J.M. Leathersich, F. Shahedipour-Sandvik, and J.M. Redwing, *J. Electron. Mater.* 41, 865 (2012).
14. J.C. Gagnon, J.M. Leathersich, F.S. Shahedipour-Sandvik, and J.M. Redwing, *J. Cryst. Growth* 393, 98 (2014).
15. G.G. Stoney and C.A. Parsons, Proc. R. Soc. Lond. A Math. Phys. Eng. Sci. 82, 172 (1909).
16. P.H. Townsend, D.M. Barnett, and T.A. Brunner, *J. Appl. Phys.* 62, 4438 (1987).
17. J.M. Hartmann, B. Gallas, J. Zhang, and J.J. Harris, *Semicond. Sci. Technol.* 15, 370 (2000).
18. W.A. Brantley, *J. Appl. Phys.* 44, 534 (1973).
19. A. Dadgar, F. Schulze, T. Zettler, K. Haberland, R. Clos, G. Straßburger, J. Bläsing, A. Diez, and A. Krost, *J. Cryst. Growth* 272, 72 (2004).
20. E.A. Fitzgerald, E.A. Fitzgerald, Y.H. Xie, D. Monroe, and P.J. Silverman, *J. Vac. Sci. Technol. B, Microelectron. Process. Phenom.* (Published for the Society by the American Institute of Physics, 1992), pp. 1807–1819.
21. W.G. Breiland, S.R. Lee, and D.D. Koleske, *J. Appl. Phys.* 95, 3453 (2004).
22. V. Srikant, J.S. Speck, and D.R. Clarke, *J. Appl. Phys.* 82, 4286 (1997).